Proceedings of Turbo Expo 2012
GT2012
June 11-15, 2012, Copenhagen, Denmark

ASME GT2012-70110

An Investigation of Applicability of Transporting Water Mist for Cooling Turbine Vanes

Reda Ragab and Ting Wang
Energy Conversion and Conservation Center
University of New Orleans
New Orleans, Louisiana, USA

ABSTRACT

This paper presents a numerical study to investigate the feasibility of transporting mist through the internal cooling channel in high-pressure turbine vanes for film cooling over the vane's surface. The idea of using mist film cooling to enhance conventional air cooling has been proven to be a feasible technique in the laboratory conditions and by computational simulations. However, there is a challenge to this technique to prove that the water mist can survive in the very hot environment inside the gas turbine casings and internal air passages and be delivered to the film injection holes. Both a zero-dimensional mist evaporation analytical model and 3-D computational fluid dynamic (CFD) scheme are employed for analysis. In the CFD simulation, the Lagrangian /Eulerian method is used along with the discrete phase model (DPM) to track the evaporation process of water droplets. The high-pressure water mist is injected into the stream of cooling air extracted from the compressor through the outer gas turbine casing near the vane before it reaches the vane internal cooling cavity. Using the mist equivalent of 10% of the cooling air mass flow rate, the results show that, when the liquid droplets are atomized to 30 μm in diameter initially, the droplets can survive inside the internal cooling passages and be delivered to the film cooling injection hole location with droplets of 20 μm in diameter; and alternatively, an initially 20 μm droplet can be delivered at 12μm in diameter, which is sufficiently large for completing the required external film cooling task.

Keywords: film cooling, mist cooling, heat transfer enhancement

NOMENCLATURE (Selected)

C_D	Aerodynamic drag coefficient.
C	Vapor concentration (kg/m^3) or Specific heat (J/kg.K)
D_{10}	Arithmetic Mean Diameter
D_{32}	Mean Sauter Diameter (ratio of droplet volume to its surface area)
h	Convective heat transfer coefficient, ($W/m^2.K$)
h_{fg}	Latent heat, (J/kg)
Nu	Nusselt number (hL/k)
P	Pressure, (Pa).
Re_d	Reynolds number (ud/ν)
Sh	Sherwood number (hL/D)
Sc	Schmidt number (ν/D)

Greek Letters

μ	Dynamic viscosity, (Pa-s)
ν	Kinematic viscosity, (m^2/s)
ρ	Density, (kg/m^3)
τ	Shear stress, (N/m^2), Time scale, (s)
ζ	Random number

Subscripts

i	Initial, Term number, Tensor index (1, 2, 3)
∞	Away from the computational cell

INTRODUCTION

Gas turbines play a vital role in today's industrialized society. As the demands for power increase, the power output and thermal efficiency of gas turbines must also increase. One method of increasing both the power output and thermal efficiency of the engine is to increase the turbine inlet temperature. In the modern advanced gas turbines, the turbine inlet temperature can be as high as 1500°C; however, this temperature exceeds the melting temperature of the metal airfoils. Therefore, it is imperative that the blades and vanes are cooled so they can withstand these extreme temperatures. Cooling air around 600K is extracted from the compressor and passes through the airfoils. With appropriate implementation of cooling schemes, the temperature of the blades can be lowered to approximately 1000K, which is permissible for reliable operation of the engine.

The film cooling technique has been applied in modern gas turbines since the 1980s to protect the hot turbine components, such as turbine blades and vanes, from hot flue gases. As there is a need to continuously increase the turbine

inlet temperature to improve gas turbine performance, continuous improvement of film cooling effectiveness is essential. There have been numerous studies that have focused on air film cooling over flat surfaces or turbine airfoil surfaces with streamwise coolant injection in the past decades (e.g., [1-3]); others have studied film cooling in airfoil cascade environments to better simulate the flow and heat transfer mechanisms at engine conditions [4-6]. While most of the above studies were conducted at the stationary cascade blades, studies on rotating turbine are also abundant. Dunn et al. [7, 8] studied the heat transfer on the vane, end walls, and rotors in a full- stage rotating turbine using a shock-tunnel facility and thin-film heat flux gages.

As the working gas temperature continuously increases to augment thermal efficiency, new cooling techniques are needed to surpass incremental improvements of convectional gas turbine cooling technologies. A promising technology to enhance film cooling is to inject water mist into the coolant flow. Each droplet acts as a cooling sink and flies over a distance before it completely vaporizes. This "*distributed cooling*" characteristic allows controlled cooling by manipulating different sizes of injected water droplets. The enhanced cooling is attributed to many factors: (a) The flow temperature is reduced mainly due to droplet evaporation and partially due to larger specific heats of water and water vapor; (b) the droplets' interactions with the flow augments turbulent mixing; (c) the sudden expansion of water vapor volume (about 900%) from fast liquid evaporation when liquid droplets touch a hot wall introduces a expulsive momentum thrust that also enhances mixing and convective heat transfer; and (d) the brief period that the liquid droplet is in contact with the hot surface provides an enhanced wall heat transfer through direct heat conduction. Another important merit of employing mist film cooling is that some larger droplets can fly longer and evaporate farther into the downstream region where the single phase air film cooling becomes less effective.

Numerous experimental and numerical investigations have been conducted on the field of air/mist cooling. One of the early experimental studies was done by Takagi and Ogasawara [9] to investigate mist/air flow and heat transfer inside a vertical rectangular tube. In this study, compressed air was mixed with water droplets generated by an atomizing nozzle before it went through the test section. Their results showed that the heat transfer coefficient decreased as the wall temperature increased. Moreover, the heat transfer coefficient increased as the droplet concentration or the air flow-rate increased or as droplet size decreased.

Mori, et al. [10] performed an experimental study of the mist/air cooling of a highly heated vertical tube of 1.8 mm ID. It was found that the heat transfer along the tube axis could be divided into three typical regions namely, liquid film region, dry-out region, and gas-phase forced convection region. In the liquid film region, the heat transfer coefficient is almost ten times higher than that without mist. In the gas-phase forced convection region, the heat transfer coefficient follows the single-phase convective heat transfer correlations. Janssen, et al. [11] performed another study on mist/air cooling of a very hot tube. The experimental setup was similar to that of Mori, et al. [10]. Experimental results demonstrated that a mixture of hot air and cold water droplets would cool a hot surface more effectively than the same mixture introduced to the same surface after the droplets have totally evaporated. These experimental results actually suggested that the droplet dynamics play an important role in the heat transfer enhancement. A heat transfer coefficient 10 times higher than that in the gas only region was also observed in the liquid film region.

Guo et al. [12, 13] studied the mist/steam flow and heat transfer in a straight tube under highly superheated wall temperatures. It was found that the heat transfer of steam could be significantly improved by adding mist into the main flow. An average enhancement of 100 % was achieved with less than 5 % mist. In another experimental study with a horizontal 180-degree tube bend, Guo et al. [14] found that the outer wall has better cooling than the inner wall. However, the inner wall can achieve better cooling enhancement. The overall cooling enhancement ranged from 40 to 300 percent with some local maximum enhancement being over 500 percent. Nazarov et al. [15] conducted experimental work investigating the heat transfer processes in cooling surfaces by a pulse gas-droplet stream. It has been shown that depending on the time parameters of the pulse spray, the integral heat transfer can effectively be controlled. They also showed that a concurrent air supply with jets, leads to an efficacious intensification of the heat transfer between the spray and a vertical obstacle. It needs to be noted that the physics of sprayed liquid jets is different from mist flow. Recently, Pakhomov et al. [16] performed a numerical simulation using the Eulerian/Eulerian method to study the flow structure and heat transfer of impact mist jet with low concentration of droplets (liquid mass flow $\leq$1 %). Their results showed that the introduction of droplets causes a substantial increase of heat transfer rate (several times) when compared with a one-phase air impact jet.

Wang, et al. [17] conducted an experimental study of a mist/steam cooling system consisting of three rows of circular jet impingement in a confined channel. The experiment results indicated that an average cooling enhancement of 200-300% was achieved with a local maximum enhancement over 800%. Nirmalan, et al. [18] applied mist/air cooling in as gas turbine vane. They found that by using mist/air cooling, the cooling airflow can be reduced more than 50% to reach the same overall cooling levels of air-only cooled vanes, but they also found that the leading-edge area is overcooled.

Because of the difficulty and cost of conducting an experiment at high Reynolds number and under elevated pressure and temperature conditions, CFD simulation has been implemented to provide preliminary flow and heat transfer physics. Many numerical studies have been performed to show the effectiveness of air/mist cooling technique. Li and Wang [19, 20] simulated mist/air film cooling and showed that a small amount of mist injection (2% of the coolant mass flow rate) could increase the adiabatic film cooling effectiveness by about 30% -50% under low temperature, velocity, and pressure conditions similar to those in the laboratory. They also investigated the

effects of different flow parameters, injection hole configurations, and coolant supply plenum on the cooling effectiveness. Both 2D and 3D film cooling geometries were simulated. Under the GT operating conditions with high temperature and high pressures, Wang and Li [21] found the mist cooling enhancement was less attractive in terms of "enhancement percentage" (10-20%) than the cases with low pressure, velocity, and temperature conditions. However, due to high surface temperature in the real gas turbine condition, a relatively smaller percentage of cooling enhancements can result in a larger wall temperature reduction, which is critical to significantly extend the life expectancy of gas turbine airfoils. To further simulate more closely to the actual GT operating conditions, Li and Wang [22] presented the mist/air film cooling heat transfer coefficient under conjugate condition by employing internal channel cooling beneath the blade surface. The results of conjugated 2-D cases indicated that reverse heat conduction from downstream to upstream along the solid wall was strong within a distance of 5 slot widths. Recently, Dhanasekaran and Wang [23] studied the effect of using mist film cooling for rotating gas turbine blades under lab and elevated (real) operating conditions. Their results showed that the average mist cooling enhancement of about 15% and 35% are achieved on the laboratory and elevated conditions, respectively. This can translate into a significant blade surface temperature reduction of 100-125 K with 10% mist injection at elevated condition.

The previous work reviewed here shows that mist cooling is a promising and efficient technique based on the assumption that the mist can be transported and delivered to the inlet of the cooling sides. However, the following questions and challenges have yet to be answered. Where is the mist generated? Can the mist survive the extremely hot conditions inside the flow passages in the gas turbine and be successfully delivered to the needed sites? The **objectiv**e of the present study is to use a CFD scheme to investigate the feasibility of transporting the mist through the internal cooling air passage to the film cooling hole sites on the vanes. This is the first paper of a series of studies to investigate how to transport mist to the needed sites, which include vanes, blades, pre-swirlers, and rotating disk cavities.

STUDIED CONFIGURATION

A schematic of a typical film cooled high- pressure turbine is shown in Fig. 1. The relatively cold compressor air (600K) is bled from the compressor discharge through the cooling air passage where it enters the cooling channels inside the turbine vanes to cool the vanes' walls, which are toasted by extremely hot flu gas at about 1300K (2350^{o}F). Eventually, the air exits the film cooling holes to form a protective layer around the external vane surface to minimize direct contact with the hot gases. Figures 2a and 2b provide a detailed view of the air flow path starting at the cooling air duct near the casing and ending at the film cooling holes at the vane surface. This path represents the computational domain of interest.

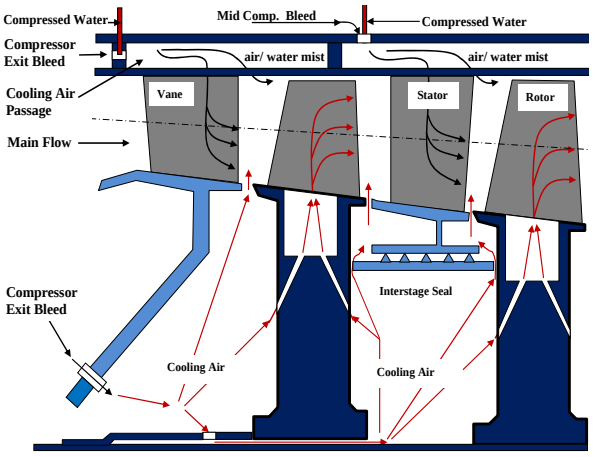

Figure 1 Schematic of mist cooling of turbine vanes using water mist injected through the Cooling air passage. (Modified from [38].)

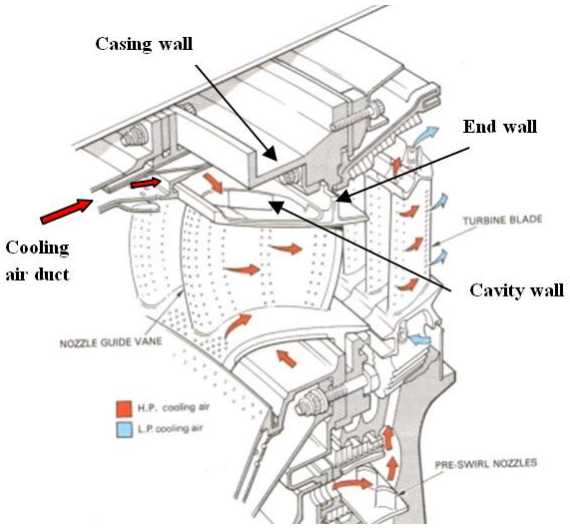

Figure 2a Cooling air flow in a high pressure turbine stage [39]

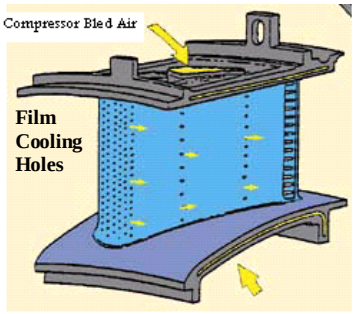

Figure 2b Schematic of turbine vane with cooling cavity (yellow) and film cooling holes. [40]

The atomizer is proposed to be located at the compressor bleed location, which is a short distance just upstream of the vane's leading edge. The water mist is to be injected at the inlet of the cooling air passage along the casing. The tubing of the high-pressure water is directly inserted through the turbine casing. For simplicity, only one

vane sector is selected for study. A more complicated arrangement or optimization strategy could be arranged in the future to reduce engineering cost and improve mist-distribution effectiveness.

ZERO-DIMENSIONAL MODEL

A quick and reasonably accurate estimate of the droplet's *residence time c*an be obtained with a simple zero-dimensional model. The residence time is the time during which the droplet starts to evaporate from the droplet surface, then boil from within the droplet, and finally become all vapor. The following correlation [24] is used to calculate the residence time (τ) of the droplet:

$$\tau = \frac{\rho_f h_{fg} d_1^2}{\lambda_1\left(1+0.23\sqrt{Re}\right)(T_1-T_f)} \qquad (1)$$

Equation 1 was derived assuming steady flow at constant pressure with the free stream temperature greater than the boiling temperature of the droplet in order for boiling to occur. It also assumes that radiation is inactive and that the droplet remains at fixed temperature (boiling temperature) throughout the boiling process. In this study, the water temperature T_f =300K, air temperature T_1= 600K, latent heat h_{fg}=2256 Kj/Kg, thermal conductivity of air λ_1=0.048 W/m.K, and droplet Reynolds no., based on droplet diameter and assumed slip velocity of 10 m/s, Re_d=55.

Based on this data, the droplet's residence time for diameters of 10 and 20 μm is calculated and shown in Table 1. The distance travelled during this period of residence time is estimated based on the cooling air velocity at 50 m/s. The results tabulated in Table 1 are very informative.

Table 1 Droplet residence time and potential traveling distance for two different sizes of water droplets

	D =10 μm	**D = 20 μm**
Time (s)	0.0072	0.0233
Distance Travelled (m)	0.358	1.169

They state that if the initial water droplets are 20 μm in diameter, their residence time is about 23 ms; and during this flashing instant, they can fly a distance greater than 1 m before they completely disappear. In a typical 7-frame GT, the distance over 1 m can cover the distance from the mist injection point to the film cooling hole base and most of the vane's surface. It is understood that, once the mist exits the film cooling holes, the droplets will face hot gas temperatures as high as 1300K. Therefore, the portion of residence time outside the vane will be shortened by about 70%. However, this quick estimate is meant to determine if the droplets can survive and reach the film cooling holes. Once they reach the cooling holes, the external film cooling behavior has been intensively studied by [12-14, 17, 19-23, 25-26, and 35-36].

It is important to emphasize that many think that the mist would disappear "instantaneously" when it is injected into the hot gas environment. Here, the above calculation informs us that this "instantaneous time" is not zero seconds, but is about 23ms for a droplet initially in 20 μm and is exposed to 600K gas. Even if the air temperature is raised to 1300K, the calculation shows that a 20 μm droplet will take 4 ms to completely evaporate, which is still not zero seconds.

Of course, this zero-dimensional analysis and associated correlation have some uncertainties, but they provide quick and positive feedback to our questions. This positive result motivates a continuous study to employ a more sophisticated multi-phase CFD scheme.

CFD CALCULATIONS

The zero-dimensional model results showed that the application of water mist/air cooling technique is feasible. To obtain more reliable results, comprehensive CFD calculations are performed for flow under real gas turbine operating conditions.

Numerical Method

A feasible method to simulate cooling with air/mist injection is to consider the droplets as a discrete phase since the volume fraction of the liquid is small (less than 0.1%). The trajectories of the dispersed phase (droplets) are calculated by the Lagrangian method (Discrete Phase Model, DPM). The impacts of the droplets on the continuous phase are considered as source terms to the governing equations of mass, momentum, energy, and species. The following are the governing equations of mass, momentum, energy and species, which are based on time averaged steady state conditions:

$$\frac{\partial}{\partial x_i}(\rho u_i) = S_m \qquad (2)$$

$$\frac{\partial}{\partial x_i}(\rho u_i u_j) = \rho g_j - \frac{\partial P}{\partial x_j} + \frac{\partial}{\partial x_i}\left(\tau_{ij} - \rho\overline{\acute{u}_i\acute{u}_j}\right) + F_j \qquad (3)$$

$$\frac{\partial}{\partial x_i}\left(\rho c_p u_i T\right) = \frac{\partial}{\partial x_i}\left(\lambda\frac{\partial T}{\partial x_i} - \rho c_p\overline{\acute{u}_i\acute{T}}\right) + \mu\Phi + S_h \qquad (4)$$

$$\frac{\partial}{\partial x_i}\left(\rho u_i C_j\right) = \frac{\partial}{\partial x_i}\left(\rho D_j\frac{\partial C_j}{\partial x_i} - \rho\overline{\acute{u}_i\acute{C}_j}\right) + S_j \qquad (5)$$

where τ_{ij} is the symmetric stress tensor. The source terms (S_m, F_j and S_h) are used to include the contributions from the dispersed phase. $\mu\Phi$ is the viscous dissipation, and λ is the heat conductivity. C_j is the mass fraction of the species (j) in the mixture, and S_j is the source term for this species. D_j is the diffusion coefficient. The diffusion term is used for bi-diffusion between water vapor and air mass. When the liquid evaporates into water vapor, it surrounds the liquid droplet. Then the water vapor will be transported away through convection and mass diffusion. Two species (air and water vapor) are simulated in the paper. The terms of $\rho\overline{\acute{u}_i\acute{u}_j}$, $\rho c_p\overline{\acute{u}_i\acute{T}}$, and $\rho\overline{\acute{u}_i\acute{C}_j}$ in the equations above represent the Reynolds stresses, turbulent heat fluxes, and turbulent concentration (or mass) fluxes, which should be modeled properly for a turbulent flow as seen in the cooling passages in gas turbines.

Generally, the Reynolds Stress Model (RSM) turbulence model performs better and is more consistent

with experimental data in mist/air or mist/steam cooling applications as reported in [25, 26]. Also, the standard k-ε turbulence model has been proven to be robust with good results only next to the RSM model [25, 26], but k-ε model required almost an order of magnitude less computational time than the RSM model does. Since the primary goal of this study is to give an estimate of the droplet residence time, the standard k-ε model is used with standard wall functions to model the near-wall turbulence structure. The mesh is generated with the first near-wall cells located y+≈30.

The equations for the turbulent kinetic energy (k) and its dissipation rate (ε) are as follows.

$$\frac{\partial}{\partial x_i}(\rho u_i k) = \frac{\partial}{\partial x_i}\left[\left(\mu + \frac{\mu_t}{\sigma_k}\right)\frac{\partial k}{\partial x_i}\right] + G_k - \rho\epsilon \quad (6)$$

$$\frac{\partial}{\partial x_i}(\rho u_i \epsilon) = \frac{\partial}{\partial x_i}\left[\left(\mu + \frac{\mu_t}{\sigma_\epsilon}\right)\frac{\partial \epsilon}{\partial x_i}\right] + C_{1\epsilon}G_k\frac{\epsilon}{k} - C_{2\epsilon}\rho\frac{\epsilon^2}{k} \quad (7)$$

The term G_k is the generation of turbulence kinetic energy due to the mean velocity gradients. The turbulent viscosity, μ_t, is calculated from the equation

$$\mu_t = \rho C_\mu \frac{\epsilon^2}{k.} \quad (8)$$

and the effective heat conductivity (λ_{eff}) and the effective diffusion coefficient are calculated by the following two equations, respectively.

$$\lambda_{eff} = \lambda + c_p\mu_t / Pr_t \quad (9)$$

$$D_{eff} = D + \mu_t / Sc_t \quad (10)$$

The constants $C_{1\varepsilon}$, $C_{2\varepsilon}$, C_μ, σ_k, and σ_ε used are: $C_{1\varepsilon}$ = 1.44, $C_{2\varepsilon}$ = 1.92, C_μ = 0.09, σ_k = 1.0, σ_ε =1.3 [27]. The turbulence Prandtl number, Pr_t, is set to 0.85, and the turbulence Schmidt number, Sc_t, is set to 0.7.

To track the trajectory of droplets, the hydrodynamic drag, gravity, and forces, such as the "virtual mass" force, thermophoretic force, Brownian force, and Saffman's lift force, are combined to affect the droplet motion. The energy equation for any individual droplet can be given as the following equation.

$$m_p c_p \frac{dT}{dt} = \pi d^2 h(T_\infty - T) + \frac{dm_p}{dt}h_{fg} + \text{Radiation} \quad (11)$$

where h_{fg} is the latent heat. The convective heat transfer coefficient (h) can be obtained with an empirical correlation [28, 29], and the radiation heat transfer term can be reasonably neglected because the extracted compressed air doesn't include combusted hot gases.

The evaporated mass is calculated by two modes: evaporation and boiling. During the evaporation mode, the evaporated mass change rate or vaporization rate is affected by the relative humidity in the air and is shown in Eq. (12) as being governed by the concentration difference between droplet surface and the air stream,

$$-\frac{dm_p}{dt} = \pi d^2 k_c(C_s - C_\infty) + \frac{dm_p}{dt}h_{fg} \quad (12)$$

where k_c is the mass transfer coefficient and C_s is the vapor concentration at the droplet surface, which is evaluated by assuming that the flow over the surface is saturated. C_∞ is the vapor concentration of the bulk flow, which is obtained by solving the transport equations. When the droplet temperature reaches the boiling point, the following equation can be used to evaluate its evaporation rate [14]:

$$-\frac{dm_p}{dt} = \pi d^2\left(\frac{\lambda}{d}\right)\left(2.0 + 0.46\,Re_d^{0.5}\right) + \ln\left(1 + c_p(T_\infty - T)/h_{fg}/c_p\right) \quad (13)$$

where λ is the gas/air heat conductivity and c_p is the specific heat of the bulk flow.

Stochastic method [30] is used to consider turbulence dispersion effect on droplets tracking. The droplet trajectories are calculated with the instantaneous flow velocity (u + u'), and the velocity fluctuations are then given as:

$$\acute{u} = \zeta\left(\overline{u'^2}\right)^{0.5} = \zeta(2k/3)^{0.2} \quad (14)$$

where ζ is a normally distributed random number. This velocity will apply during the characteristic lifetime of the eddy (t_e), a time scale calculated from the turbulence kinetic energy and dissipation rate. After this time period, the instantaneous velocity will be updated with a new ζ value until a full trajectory is obtained. Since the results are sensitive to the time scale, an appropriate selection of the time scale is critical. In this study, the time scale is selected as 0.009 (k/ε). More detailed study about the effect of time scale on computational results and an appropriate selection of time scale is referred to [26].

Computational Domain

The computational domain is a part of the cooling passage that feeds the vane with the cooling air besides the cooling cavity inside the vane. As the Frame 7FA engine contains 48 vanes in the first turbine stage, the computational domain is a sector of 360/48 = 7.5° in the circumferential direction. The part simulated from the air cooling passage is 25 cm in the axial direction, which represents 1.25 the vane axial chord length with a height of 7 cm. The vane cooling cavity (channel) is approximated to be a cylinder with a 5 cm diameter and a height of 18 cm equal to that of the vane. The exit of the domain is a row of film cooling holes that contains 28 holes in the radial direction (z-direction) with 0.15 cm in diameter for each. The computational domain is shown in Fig. 3 with red arrows representing the cooling air flow direction. The water mist is injected at the inlet of the cooling passage and moves with the air until the droplets reach the exit holes.

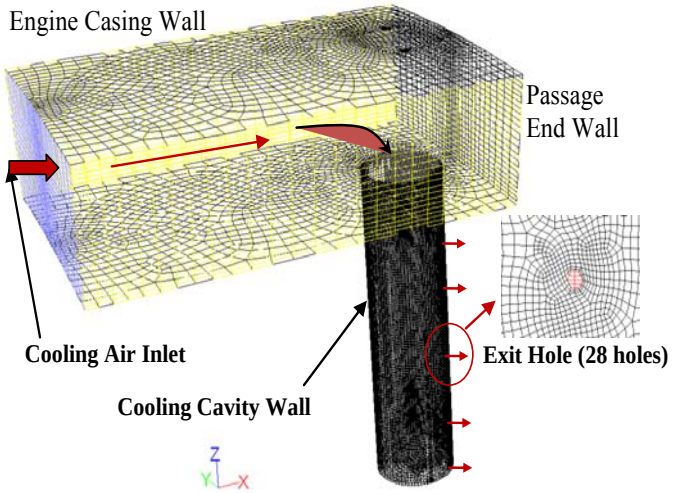

Figure 3 The computational domain

Boundary Conditions

Airflow

The main flow is assumed to be dry air (zero humidity). The mist cooling is investigated at real working conditions of a Frame7 FA gas turbine engine. As a single row of film cooling holes is used, the mass flow rate is calculated as a 1.6 % of the engine total mass flow rate. This mass flow is divided among the 48 nozzles to give an inlet mass flow rate of 0.1483 kg/s, which is imposed on the inlet boundary. The inlet static temperature is 600 K, reasonably assumed equal to the compressor discharge temperature. Inlet turbulence conditions for k and ε are defined according to the following correlations:

$$k = \frac{3}{2}\left(u_{avg} I\right)^2 \quad (15)$$

$$\epsilon = C_\mu^{3/4} \frac{k^{3/2}}{\ell} \quad (16)$$

$$\ell = 0.07\, D_h\,, \quad (17)$$

where the turbulence intensity I = 5% is assigned to simulate a fully-developed duct flow; the turbulence length scale, ℓ, is based on the inlet hydraulic diameter of the air cooling duct D_h = 9.12cm; C_μ = 0.09; u_{avg} is the average inlet air velocity.

For the cooling passage along the outer casing and feeding the vane cavity, the side walls in the circumferential direction are assumed symmetric with zero normal gradients; the bottom wall has a constant temperature of 1100 K as it is adjacent to the hot flue gases about 1300K; and the upper and end walls are assumed adiabatic. For the cooling cavity walls, the temperature is taken as 900 K in the baseline case. All walls are assumed to be no-slip walls. At exit of the domain, which is a vertical row containing 28 holes, a constant static pressure of 16 atm is imposed along the boundary. This pressure represents the actual pressure of the flue gases in the main stream felt by the film cooling holes. These boundary conditions are summarized in Table 2.

Table 2 Boundary conditions

Boundary	Values Assigned
Inlet	Mass flow rate = 0.01483 kg/s T = 600 K, I=5 %, D_h = 9.12 cm
Exit	Static Pressure = 16 atm
Sides	Symmetric with zero normal gradients
Walls	No-Slip, Lower passage wall at 1100 K Cavity wall temperature = 900 K

Droplet Injection

The uniform droplet size of 30μm is considered in the base case (Table 3) with injection velocity of 1.05 m/s (equal to the mass weighted average velocity of the air flow at inlet); and the mist ratio, the mass ratio of mist over cooling airflow, is 10% (about 0.01483 kg/s) in the base case. The number of mist injection points at the coolant inlet depends on the number of computational elements (cells) at the inlet surface. In the present case, about 8160 injection points are placed. The trajectory number for stochastic tracking is chosen to be 10.

Table 3 Base case conditions

Parameter	Value
Air (Dry base Case)	
Air inlet mass Flow	0.1483 kg/s
Air inlet temperature	600 K
Exit static pressure	16 atm
Cavity wall temperature	900 K
Turbulence model	Standard k-ε
Droplets (Wet base case)	
Droplet initial diameter	30 μm
Droplet initial velocity	1.05 m/s
Droplet initial temperature	300 K
Mist Ratio	10 %
Droplet wall boundary cond.	Reflect

Discrete-phase wall boundary condition

When the droplet reaches the wall, its trajectory is determined from the discrete-phase wall boundary condition. There are many possible trajectories that a droplet can take; and each droplet, as it approaches the wall, has a particular trajectory [30] based on whether the wall is dry or flooded. In the case of a dry wall, the droplets have three major regimes, including reflect, break-up, and trap. According to Watchers et al. [31], the regimes depend on the incoming Weber number of the droplet. Here, the Weber number is the ratio of kinetic energy of the droplet to its surface tension energy ($We = \rho D V_d^2/\sigma$). It was shown from their experimental results that the droplet with an incoming Weber number (We_{in}) less than 10 reflects elastically with a nearly equal outgoing Weber number (We_{out}). As the incoming We increased further to $We_{in} > 80$, the droplet falls into disintegration region which leads to breakup of the

droplet to several small droplets. In the transition region of 30<We<80, the droplet has the possibility of either reflecting or breaking-up. Apart from the above two facts, the droplets can be instantaneously vaporized by the superheated wall also. In this case, the trajectory calculations are terminated and particles' entire mass passes into the vapor phase and enters the cell adjacent to the boundary. On the other hand, in the presence of a flooded wall condition, a droplet has the chance for four different regimes, including splashing, spreading, rebounding, or sticking. For the spread regime, the arriving drops are assumed to coalesce to form a local film. The *wall-film* boundary condition used in this study is based on the work of Stanton et al. [32] and O'Rourke et al. [33]. The four regimes — stick, rebound, spread, and splash — are based on the impact energy and wall temperature. Below the boiling temperature of the liquid, the impinging droplet can stick, spread, or splash; however, while above the boiling temperature, the particle can only either rebound or splash. The impact energy is defined by

$$E^2 = (\rho V_r^2 D/\sigma) [1/(\min (h_0 /D ,1) + \delta_{bl} /D] , \qquad (18)$$

where V_r is the relative velocity of particle in the frame of the wall, δ_{bl} is the boundary layer thickness, D is the droplet diameter, σ is the droplet surface tension, and h_0 is the film thickness.

The sticking regime is applied when the value of E becomes less than 16. Splashing occurs when the impingement energy is above a critical E value of $E_{cr} = 57.7$. More details about the wall-film model can be found in [32, 33]. In addition to the *reflect* and the *wall-film* boundary conditions, there is a commonly used boundary condition known as the *wall-jet* model and it is based on the work of Naber and Reitz [34]. The *wall-jet* boundary condition is appropriate for high-temperature walls where no significant liquid film is formed, and in high-Weber number impacts where the spray acts as a jet. The wall-jet boundary condition assumes an analogy with an inviscid jet impacting a solid wall where the outcome of impingement (the direction and velocity of the droplet) depends mainly on the droplet Weber number and on its impingement angle. According to the value of Weber number, the droplet may reflect (We < 80) or slide along the wall (We>80). A more detailed description of the underlying theory of that model is available in [34]. The boundary condition of droplets at walls in the base case is assigned as "reflect," which means the droplets elastically rebound once reaching the wall.

The droplets are injected with a velocity equal to that of the inlet air and a temperature of 300 K. The details of base case conditions are given in Table 3. To further understand the effect of some important operating parameters, a parametric study is performed as shown in Table 4. The parameters chosen for study are droplet initial diameter (D_i), the mist ratio, the cavity wall temperature ($T_{w)}$, and the droplet boundary condition at the wall. The results of the parametric study are shown in the results section of this paper. At the outlet, the droplets just simply escape from the computational domain (exit holes).

Table 4 The matrix of the parametric study

Case	D_i (μm)	Mist ratio (%)	T_w (K)	Droplet BC
1	20			
Base case	**30**	**10**	**900**	**Refelct**
2	40			
3		5		
Base case	**30**	**10**	**900**	**Refelct**
4		15		
5			800	
Base case	**30**	**10**	**900**	**Refelct**
6			1000	
7				Wall-jet
Base case	**30**	**10**	**900**	**Reflect**
8				Wall-film

Meshing and Simulation Procedure

The computational domain is constructed by unstructured hexahedral elements as shown in Fig. 3. This type of cell falls between the structured hexahedral and the unstructured tetrahedral in terms of the accuracy of the solution obtained. The computational domain geometry is decomposed into 5 sub-regions before being meshed with the Cooper scheme that yields this kind of mesh. More intensive meshes are used near the walls, especially the cavity walls and the film holes, in order to give a value of y^+ ≈30 which is reasonable for the turbulence model selected.

Four mesh densities are tested for grid independence, and the base case is solved for every mesh. The results are compared and summarized in Table 5 for selection of the appropriate mesh size.

Table 5 Grid independency analysis

	50K Cells	**100K Cells**	**211K Cells**	**460K Cells**
Dry Exit Static Temperature (K)	621.9	609.7	611.8	608.2
Max. Predicted Residence Time (s)	0.398	0.378	0.427	0.434
D_{10} (μm)	18.96	18.99	18.93	18.32
D_{32} (μm)	21.03	21.06	20.98	20.94

Actually, all solution variables give the same trend but only selected ones are presented here. For the dry case, the most relevant solution variable is the static temperature of the air at the film holes, so mass weighted average value over all holes is selected as a criterion for the comparison. For the wet case (with droplets), residence time, arithmetic mean diameter (D_{10}), and Sauter mean diameter (D_{32}) are the selected variables to be monitored. Comparing the variable values at the last two columns of Table 5, it can be seen that the solution has achieved variations within 0.1%-3% between the last two mesh sizes. This suggests that the grid of 211,000 cells gives the cost-effective choice and hence, it is used for the remaining parametric study.

The simulation is carried out using the commercial CFD software ANSYS12.0 from Ansys, Inc. The simulation uses the segregated solver, which employs an implicit

pressure-correction scheme and decouples the momentum and energy equations. The SIMPLE algorithm is used to couple the pressure and velocity. Second order upwind scheme is selected for spatial discretization of the convective terms and species. The computation is conducted for the main and coolant flow field (continuous phase) first. After obtaining an approximate converged flow field of the air, the dispersed phase of droplet trajectories are calculated. At the same time, drag, heat, and mass transfer between the droplets and the air are calculated. Iterations proceed alternatively between the continuous and discrete phases. Converged results are obtained after the residuals satisfy mass residual of 10^{-3}, energy residual of 10^{-6}, and momentum and turbulence kinetic energy residuals of 10^{-4}. These residuals are the summation of the imbalance for each cell, scaled by a representative of the flow rate.

RESULTS AND DISCUSSION

Model Validation

The mist/steam cooling CFD scheme and model have been validated by the same research group members Dhanasekaran and Wang [25-26, 35-36] with the experimental data in conditions like flow in heated tubes [12,13], 180-degrees tube bend [14], and impinging jets [17]. The mist/air cooling CFD models have been qualified by Li and Wang [19-22]. The same CFD scheme and model are used in this study, hence no validation is repeated here.

Base Case Results

In the current work, a numerical simulation is performed with the base case conditions shown in Table 3. The flow field in the dry base case is solved first without droplets until a converged solution is obtained then the droplets are injected according to specifications in Table 3 for the mist base case. Figures 4 and 5 show the static temperature contours at a mid-plane for the dry and mist base cases, respectively.

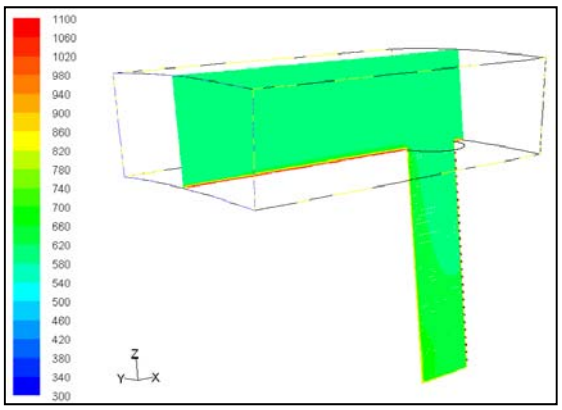

Figure 4 Contours of the static temperature (K) at the mid-plane in the dry base case (No water mist is injected)

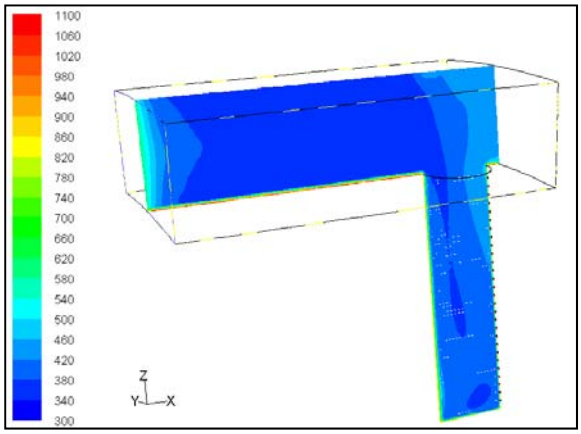

Figure 5 Contours of the static temperature (K) at the mid-plane in the mist base case (10% Mist Ratio, 30 μm initial droplet diameter, 900 K cavity wall temperature)

Due to the droplets evaporation and boiling, latent heat of vaporization is absorbed from the main flow resulting in a remarkable reduction, approximately 200 degrees, in the air temperature. This is a very important result as it implies a high cooling potential for the mist cooled cavity air. As the air temperature is reduced, the amount of air required for cooling the engine components, which is bled from the compressor, can be notably reduced and the net output power can be augmented. Also, saving the precious compressor air helps to increase the thermal efficiency of the gas turbine engine. Another factor that leads to savings in the compressor air is that the specific heat of air/water vapor mixture is higher than that of air alone. This means a higher cooling capacity of the mist-air and hence a lower compressed air consumption. The final contribution from the mist comes from its higher film cooling effectiveness which can help extend the life of the turbine components.

Figure 6 shows the contours of water vapor mass fraction from the evaporation and boiling of the droplet streams under the base case conditions.

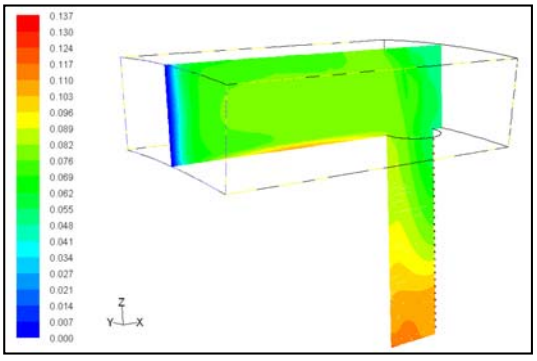

Figure 6 Contours of the mass fraction of water vapor at the mid-plane in the mist base case

Figures 7 and 8 show the droplet traces colored by droplet diameter (cm) and droplet residence time (s), respectively. It can be noticed that trajectories close to the wall vanish early in the domain. A thin layer of water vapor

with high Cp value is therefore formed and shields the core flow from the hot wall, thus leaving the core flow cooler to sustain the water droplets longer. *This key result supports the zero-dimensional result that droplets can survive up to the exit cooling hole*s. Again, the main goal of the current study is to prove that droplets with reasonable diameters and loading can survive in this very hot environment until they reach the cooling holes. Moreover, the droplets that exit the cooling holes should be of sufficient mass (or diameter) to sustain the mist cooling over the external vane surface. Please note that not all of the droplet streams are shown in Figs. 7 and 8. The CFD solution helps show the flow behavior in the cooling cavity up to the cooling holes. It is noticed that the number of droplet trajectories is low at the upper 7 holes. This happens as a result of the flow separation in the vicinity of the inlet region of the cooling cavity. This flow separation happens due to the presence of the stagnation zone near the "end wall" at the end of the air cooling duct. This separation region deflects the droplets away from the cavity wall for the upper 7 holes. This problem can be mitigated by designing a tapered end wall if so designed.

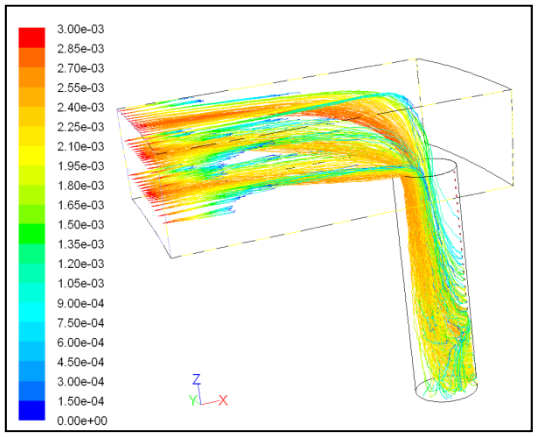

Figure 7 Droplet traces colored by droplet diameter (cm) in the base case (10% Mist Ratio, 30 µm initial diameter, 900 K cavity wall temperature)

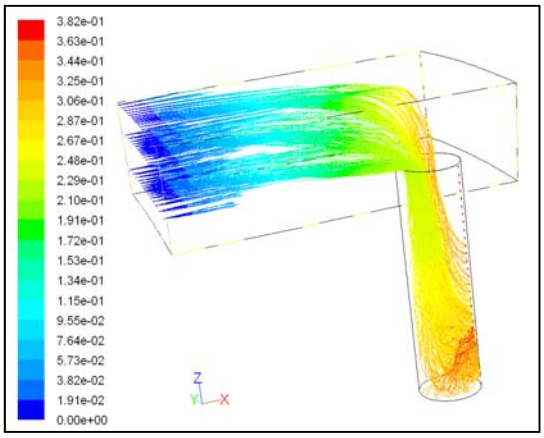

Figure 8 Droplet traces colored by residence time (S) in the base case (10% Mist Ratio, 30 µm initial diameter, 900 K cavity wall temperature)

Figure 9 shows the droplet diameter distribution at exit holes in the base case. The mean droplet diameter can be evaluated in various ways. The most commonly used mean diameters are the Arithmetic Mean Diameter, D_{10}, and the Sauter Mean Diameter, D_{32}. Both diameters can be defined as follows:

$$D_{10} = \frac{\sum_{i=1}^{n} d_i}{n}, \quad D_{32} = \frac{\sum_{i=1}^{n} d_i^3}{\sum_{i=1}^{n} d_i^2} \qquad (19)$$

Where n is the total number of droplets. The Sauter mean diameter is of interest in applications where the active surface area is important, as in spray evaporation applications. Droplets with arithmetic mean diameter of 18.93 µm and mean Sauter diameter of 20.98 µm are obtained. These diameters are suitable for mist/film cooling over the external vane surface as previously studied by References 9-13

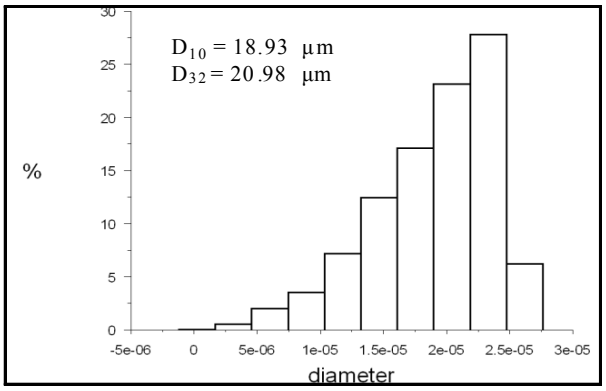

Figure 9 Diameter [m] distribution histogram at exit holes in the base case (10% Mist Ratio, 30 µm initial diameter, 900 K cavity wall temperature)

Parametric Study

The required outcome of this work is to prove the existence of droplet streams with reasonable diameters (in the order of 15-20 µm) at film holes. To understand well the effect of changing operating parameters on the droplet distribution at the exit, a parametric study is performed. Mist ratio (ratio of the mass flow rate of water mist to the air mass flow), initial mean diameter of injected droplets, cavity wall temperature, and wall droplet boundary condition are the studied parameters. Although the real droplet diameters are polydispersed, all the cases are performed assuming a uniform (monodispersed) droplet diameter distribution. This simplification is necessary for exercising a controlled study to track change of droplet's size. To show the effect of injected diameter distribution, one case is calculated with injected droplet diameters follow the Rosin-Rammler distribution [20].

Effect of Changing Injection Mist Ratio

Particle loading is an important parameter in any two-phase flow application. Mist ratio, defined as the ratio of mass flow rate of water mist at injection location to that of air, is used here to express the effect of particle loading. As shown in Figs. 10 and 11, reducing the mist ratio from 10% to 5% causes almost all the droplets to evaporate leaving

only 2 droplet streams out of 8160 to reach the exit holes. This is clearer in Fig. 12, where the mean droplet diameter at exit is reduced to 1.71 µm compared with 21.26 µm at 15 % mist ratio. This suggests that at least 10 % mist ratio is required for Frame 7FA gas turbine vanes to provide the necessary amount of mist that can be used for film cooling.

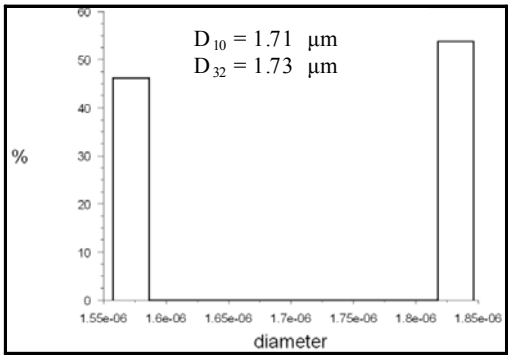

Figure 10 Diameter [m] distribution histogram at exit holes with 5% Mist Ratio

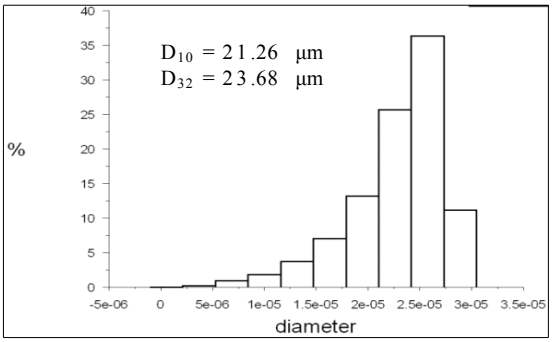

Figure 11 Diameter [m] distribution histogram at exit holes with 15% Mist Ratio

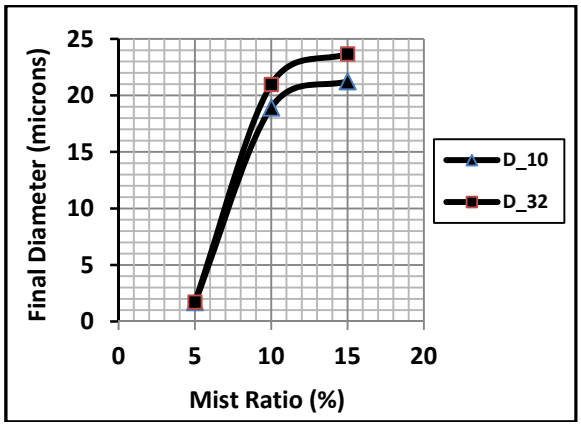

Figure 12 Effect of changing Mist Ratio (%) on droplet exit diameter.

Effect of Changing Injection (Initial) Diameter

As shown in Figs. 13 and 14, injecting 10% mass ratio of droplets with initial diameters 30µm (or larger) is necessary to get 20 µm (or larger) at exit holes. This trend is clearer in Fig. 15, where the mean droplet diameter at exit increases to 25.77 µm with initial droplet diameter of 40 µm compared with 12.65 µm in final average droplet diameter with 20 µm initial diameter. Also, the relation between the initial and final diameters seems to be linear, as shown in Fig. 5 with a linearity constant of approximately 0.628 for the arithmetic mean.

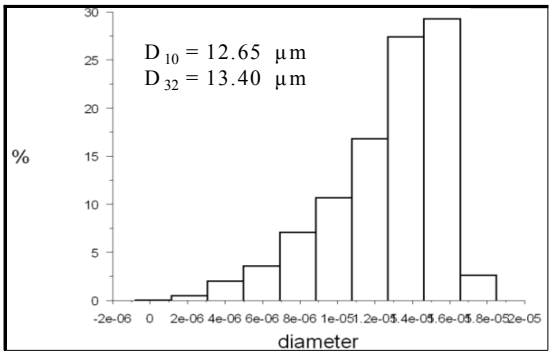

Figure 13 Diameter [m] distribution histogram at exit holes with 20 µm initial diameter

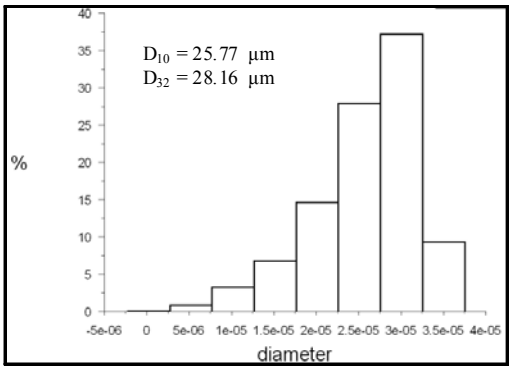

Figure 14 Diameter [m] distribution histogram at exit holes with 40 µm initial diameter.

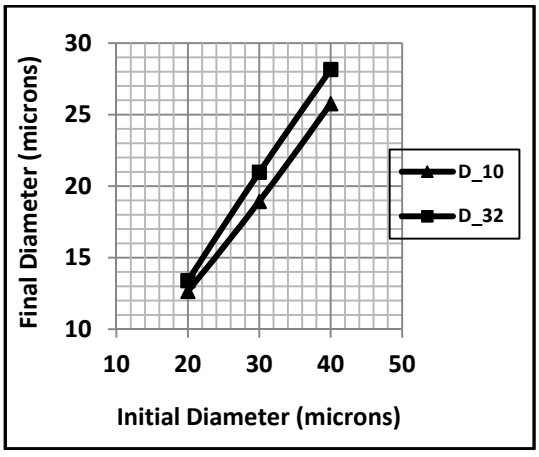

Figure 15 Effect of changing droplet injection (Initial) diameter on droplet exit diameter

A similar situation happens for the mean Sauter diameter. This can help in estimation of the required inlet diameter to achieve a certain cooling effect associated with a certain exit diameter. These results suggest that droplets with diameters ranging from 30-20 μm and a mist mass ratio of 10% are suitable to achieve the droplet sizes in the range of 10-20 μm that are more effective in mist/film cooling for Frame 7FA gas turbine vanes. This diameter range is suitable from heat and mass transfer point of view as it enables the droplets to survive until they reach the exit holes and complete their trip around the vane external surface. From the aerodynamics point of view, this diameter range has a small Stokes number, which means that it will follow the main stream and reduce its chances of impinging at walls. This in turn would reduce the concerns of erosion and localized thermal stresses, but more detailed study needs to be conducted to draw a conclusion with more certainty.

Effect of Changing Cavity Wall Temperature

In real gas turbines, the blade cooling process is a complex conjugate heat transfer problem. Hence, the cavity wall temperature depends on both the internal flow cooling and heating from the external flows along with the wall material. A more precise way is to calculate the flow fields and heat transfer both inside and outside the walls. However, since the present study is only focused on the droplet evaportation in the interal flow, the wall temperature has been assigned as a boundary condition. Since the conjugate heat trasnfer problem is not solved, a range of wall temperature between 1000K and 800 K is hereby assigned to bracket the wall temperature that could occur in the real condition. The results of droplet diameter distribution at exit holes are shown in Fig. 16. It can be concluded that the droplet diameter reduces within 1μm with the increase of cavity wall temperature from 800K to 1000K.

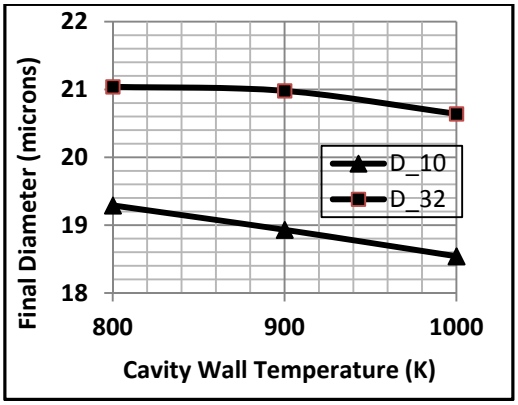

Figure 16 Effect of changing cavity wall temperature on droplet exit diameter

Effect of Changing Wall Droplet Boundary Condition

Generally, wall boundary condition plays a significant role in droplet trajectory calculation in wall- bounded flows. As the droplet hits the wall, the droplet encounters a change in velocity and/or direction according to the wall boundary condition selected. In the base case, the simple *reflect* boundary condition was selected. This boundary condition calculates the reflection angle of the droplet based on its incidence angle assuming that velocity remains unchanged, i.e., elastic impaction. The results of the base case are presented earlier in Fig. 9. In the parametric study, another two boundary conditions are used, namely, *wall-film* and *wall-jet* boundary conditions with the details of those models discussed earlier. The results show that the droplets' diameter distribution at exit in the wall-film and wall-jet boundary conditions cases are almost identical to that of using the reflect wall condition as shown in Fig. 9. The averaged diameters of the three conditions are almost identical, as compared in Fig. 17. It can be concluded that the droplet boundary condition at the wall has a negligible effect on the droplet diameter distribution at exit which is expected in the current work. As the wall is highly superheated and at a much greater temperature than the water boiling temperature, it is unlikely to have a wall-film forming on it due to the deposition or sticking of water droplets [32-33]. Therefore, it is not unexpected that different droplet wall boundary conditions do not render results that differ by very much.

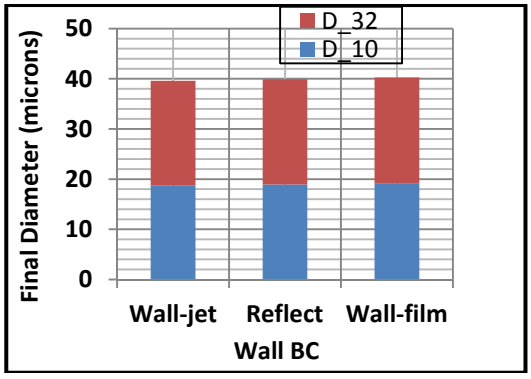

Figure 17 Effect of changing wall droplet boundary condition on droplet exit diameter distribution

Effect of Droplet Initial Diameter Distribution

The effect of droplet diameter distribution at inlet is studied by first injecting uniform diameters of 20, 30, and 40 μm, respectively, to gain a clear understanding of the droplet size effect under a controlled condition. This is followed by injecting distributed droplet diameters to simulate more closely the actual atomized droplet condition. The Rosin-Rammler distribution function [37] is used based on the assumption that an exponential relationship exists between the droplet diameter, d, and the mass fraction of droplets with diameter greater than d as follows:

$$Y_d = e^{-(d/d_m)^n} \qquad (20)$$

where d_m refers to the mean diameter 30 μm and n refers to the spread parameter. From the relationship, the spread parameter of 5.94 is calculated and used to fit the size distribution into the CFD model. Basically, five diameter sets are used to express the whole range of droplets, and a spread parameter, n, is calculated for each set from using Eq. (20). An average value of 5.94 is obtained from Eq. 20 as the

spread parameter in the current study. The result of using the Rossin-Rammler distribution as the initial droplet size distribution in Fig. 18 shows that droplet distribution at exit tends to be closer to the larger diameter case. This happens because smaller diameters in the distribution (from 0 to 30 μm) tend to evaporate quickly leaving only the droplets with larger diameters to survive the journey.

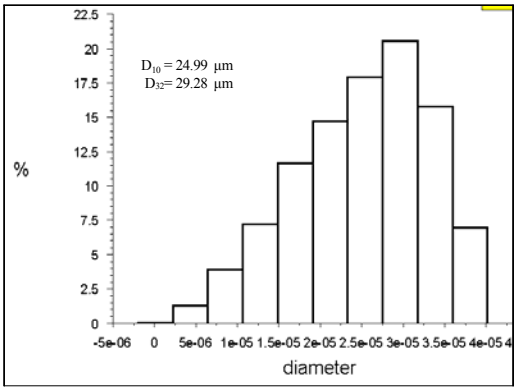

Figure 18 Diameter[m] distribution histogram at exit holes with Rossin-Rammler initial diameter distribution

CONCLUSIONS

From the current investigation, some conclusions can be drawn as follows:

- The mist cooling for high-pressure gas turbine vane is feasible under real operating conditions.
  For example, under real Frame 7FA operating conditions, 50% of the mist can survive with an average droplet diameter of 10 – 20 μm if mist with 10% mass ratio and 20-30μm in initial diameter is injected.
- Due to the large superheated wall temperature, a thin layer of water vapor with higher Cp value than air is formed near the wall. This vapor layer shields the core flow from the hot wall, thus leaving the core flow cooler to sustain the water droplets flying longer.
- The relation between the initial and final injected diameters is found to be linear, while the relation between mist ratio and final diameter is not. This gives some control of the operating conditions of the mist cooling technique.
- The effect of different wall droplet boundary conditions was found inconsequential.

The results obtained in this study are very encouraging and warrant a continuous study to find a method to transport the mist to the rotating blade. Furthermore, the mist-induced cooling enhancement may introduce local cold spots of overcooling. Therefore, development of a coupled multi-phase CFD model and finite-element stress analysis will be a future task.

ACKNOWLEDGEMENT

The authors want to thank Louisiana Governor's Energy Initiative to support this project via the Louisiana Board of Regents and the Clean Power and Research Energy Consortium (CPERC).

REFERENCES

[1] Goldstein, R. J., 1971, "Film Cooling : Advances in Heat Transfer," Vol. **7**, Academic Press, New York, pp. 321–379.

[2] Mayhew, J. E., Baughn, J. W. and Byerley, A. R., 2003, "The Effect of Freestream Turbulence on Film Cooling Effectiveness", Int. J.Heat Fluid Flow, Vol. 24, pp. 669-679.

[3] Walters, D. K. and Leylek, J. H., 1997, "A Detailed Analysis of Film-Cooling Physics-Part 1: Streamwise Injection with Cylindrical Holes", ASME Paper No. 97-GT-269, Proceedings of the ASME Turbo Expo 1997, Orlando, FL, USA, June2-5, 1997.

[4] Zhang, L. J. and Pudupaty, R., 2000, "The Effects of Injection Angle and Hole Exit Shape on Turbine Nozzle Pressure Side Film Cooling,"ASME Paper No. 2000-GT-247 , Proceedings of the ASME Turbo Expo 2000, Munich, Germany, May 8-11, 2000.

[5] Drost, U. and Bolcs, A., 1998, "Investigation of Detailed Film Cooling Effectiveness and Heat Transfer Distributions on a Gas Turbine Airfoil", ASME Paper No. 98-GT-20, Proceedings of the ASME Turbo Expo 1998, Stockholm, Sweden, June1-4, 1998.

[6] Medic, G., and Durbin, P. A., 2002, "Toward Improved Film Cooling Prediction", ASME J.Turbomach., Vol. 124, pp. 193–199.

[7] Dunn, M.G., 1986, "Heat Flux Measurement for a Rotor of a Full Stage Turbine. Part I: Time averaged Results", ASME Journal of Turbomachinery, Vol. 108 (1), pp.90-97.

[8] Dunn. M.G., George, W.K., Rae, W.J., Woodward, S.H., Moller, J.C. and Seymour, J.P., 1986, "Heat Flux Measurement for a Rotor of a Full Stage Turbine, Part II: Description of Analysis Technique and Typical Time-Resolved Measurements", ASME Journal of Turbomachinery, Vol. 108 (1), pp.98-107.

[9] Takagi, T. and Ogasawara, M., 1974, "Some Characteristics of Heat and Mass Transfer in Binary Mist Flow," Proceedings of 5th Intl. Heat Transfer Conf., Tokyo, No. 4, pp.350-354.

[10] Mori, Y., Hijikata, K. and Yasunaga, T., 1982, "Mist Cooling of Very Hot Tubules with Reference to Through-Hole Cooling of Gas Turbine Blades," Intl. J. Heat Mass Transfer, Vol 25, No.9, pp.1271-1278.

[11] Janssen, J.M., Florschuetz, L.W. and Fizdon, J.P., 1986, "Heat Transfer to Two-Phase Air/Water Mixtures Flowing in Small Tubes with Inlet Disequilibrium," NASA CR 175076.

[12] Guo, T., Wang, T., and Gaddis, J. L., 2000, ''Mist/Steam Cooling in a Heated Horizontal Tube Part I: Experimental System,'' ASME J. Turbomach., Vol. 122, pp. 360–365.

[13] Guo, T., Wang, T., and Gaddis, J. L., 2000, ''Mist/Steam Cooling in a Heated Horizontal Tube:

Part II: Results and Modeling,'' ASME J. Turbomach., Vol. 122, pp. 366–374.
[14] Guo, T., Wang, T., and Gaddis, J. L., 2000, ''Mist/Steam Cooling in a 180-Degree Tube,'' ASME J. Heat Transfer, Vol. 122, No. 4, pp. 749–756.
[15] Nazarov, A. D., Serov, A. F., Terekhov, V. I., and Sharov K. A., 2009,"Experimental Investigation of Evaporative Pulse-Spray Impingement Cooling," J. of Eng. Physics and Thermophysics, Vol. 82, No. 6, pp. 1184-1190.
[16] Pakhomov, M. A., and Terekhov, V. I., 2010,"Enhancement of an Impingement Heat Transfer between Turbulent Mist Jet and Flat Surface," Int. J. of Heat and Mass Transfer, Vol. 53, pp. 3156-3165.
[17] Wang, T., Gaddis, J. L., and Li, X., 2005," Mist/steam Heat Transfer of Multiple Rows of Impinging Jets," Int. J. Heat and Mass Transfer, Vol. 48, pp. 5179-5191.
[18] Nirmalan, N.V., Weaver, J.A. and Hylton, L.D., 1996, "An Experimental Study of Turbine Vane Heat Transfer with Water-Air Cooling," ASME paper No. 96-GT-381, Proceedings of the ASME Turbo Expo 1996, Birmingham, UK, June 10-13, 1996.
[19] Li, X. and Wang, T., 2006, "Simulation of Film Cooling Enhancement with Mist Injection", ASME Journal of Heat Transfer, Vol. 128 (6), pp.509-519.
[20] Li, X., and Wang, T, 2007, "Effects of Various Modeling on Mist Film Cooling", ASME Journal of Heat Transfer, Vol. 129, pp. 472-482.
[21] Wang, T., and Li, X., 2008, "Mist Film Cooling Simulation at Gas Turbine Operating Conditions", International Journal of Heat and Mass Transfer, Vol. 51, pp. 5305-5317, 2008.
[22] Li, X., and Wang, T., 2008, "Two-Phase Flow Simulation of Mist Film Cooling on Turbine Blades with Conjugate Internal Cooling", ASME Journal of Heat Transfer, Vol. 130, pp.102901/1-8
[23] Dhanasekaran, T. S., and Wang, T., 2009, "Simulation of Mist Film Cooling on Rotating Gas Turbine Blades," ASME Paper No. GT2009-59424.
[24] Kuo, K. Y., 1986, "Principles of combustion," John Wiley and Sons, New York.
[25] Wang, T. and Dhanasekaran, T. S., 2010, "Calibration of a Computational Model to Predict Mist/Steam Impinging Jets Cooling in Gas Turbine Blades," ASME Journal of Heat Transfer, Vol. 132, Isu. 12, 122201/1-11, 2010
[26] Dhanasekaran, T. S. and Wang, T., 2008, "Validation of Mist/steam Cooling CFD Model in a Horizontal Tube," ASME paper HT08-56280, Proceedings of the ASME 2008 Summer National Heat Transfer Conference, August 10-14, 2008, Jacksonville, FL, USA
[27] Launder, B. E. and Spalding, D. B., 1972,"Lectures in Mathematical Models of Turbulence," Academic Press, London, England.
[28] Ranz, W. E. and Marshall Jr. W. R., 1952, "Evaporation from Drops Part I", Chem. Eng. Prog, Vol. 48, pp. 141-146.
[29] Ranz, W. E. and Marshall Jr, W. R., 1952, "Evaporation from Drops, Part II, Chem. Eng. Prog, Vol. 48, pp. 173-180.
[30] ANSYS Manual, Version 12.0, 2009, Ansys Inc.
[31] Watchers, L. H. J., and Westerling, N. A., 1966, "The Heat Transfer from a Hot Wall to Impinging Water Drops in the Spherioidal State," Chem. Eng. Sci., 21, pp. 1047-1056.
[32] Stanton, D. W., and Rutland, C. j., 1996, "Modeling Fuel Film Formation and Wall Interaction in Diesel Engines," SAE Paper 960628.
[33] O' Rourke, P. J. O., and Amsden, A. A., 2000, "A Spray/Wall Interaction Submodel for the KIVA-3 Wall Film Model," SAE Paper 2000-01-0271.
[34] Naber, J. D, and Reitz, R. D., 1988, "Modeling Engine Spray/Wall impingement ," Technical Repoprt 880107, SAE, General Motors Research Laboratories, Warren, MI.
[35] Dhanasekaran, T. S. and Wang, T., 2010, "CFD Model Validation and Prediction of Mist/Steam Cooling in a 180-Degree Bend Tubes," Proceedings of the 14th International Heat Transfer Conference, paper IHTC14-22833, August 8-13, 2010, Washington D.C.
[36] Dhanasekaran, T. S. and Wang, T., 2011, "Mist/air Cooling in a Two-Pass Rectangular Rotating Channel with 45-deg Angled Rib Turbulators," ASME Paper No. GT2011-45954, Proceedings of ASME Turbo Expo2011, Vancouver, Canada, June 6-10, 2011
[37] Rosin, P., and Rammler, E., 1933, "The Laws Governing the Fineness of Powdered Coal," Journal of the Institute of Fuel, Vol. 7, Oct. 1933, pp. 29-36.
[38] Kurzke, J., 2007 "Gas Turbine Details 5" http://www.gasturb.de/Free/Manuals/GasTurbDetails5.pdf
[39] Oldfield, M., 2007, "Keep it Cool! 38 years of Gas-Turbine Research," A lecture given on 15 Sept., 2007, www.soue.org.uk/souenews/issue7/osney.html
[40] Dennis, R. 2006, "The Gas Turbine Handbook," U.S. Department of Energy.